

Optical Analogy to Electronic Quantum Corrals

G erard Colas des Francs and Christian Girard

Centre d'Elaboration des Mat eriaux et d'Etudes Structurales (CNRS), 29 rue J. Marvig, F-31055 Toulouse, France

Jean-Claude Weeber, C edric Chicane, Thierry David, and Alain Dereux

Laboratoire de Physique de l'Universit e de Bourgogne, Optique Submicronique, 9 avenue A. Savary, F-21011 Dijon, France

David Peyrade

Laboratoire de Microstructures et Micro electronique (CNRS), 196 Avenue H. Ravera, F-92225 Bagneux, France

(Received 27 November 2000)

We describe full multiple-scattering calculations of localized surface photonic states set up by lithographically designed nanostructures made of a finite number of dielectric pads deposited on a planar surface. The method is based on a numerical solution of the dyadic Dyson's equation. When the pads are arranged to form a closed circle, we find field patterns that look like the electronic charge density recently observed above quantum corrals. We propose two experimental techniques that could be used to observe these electromagnetic modes in direct space.

DOI: 10.1103/PhysRevLett.86.4950

PACS numbers: 82.37.Gk, 78.67.-n, 78.68.+m

The surface limiting a solid body is well known to modify locally the physical properties of many materials (dielectric, metal, or semiconductor) [1]. The interface breaks the full translation symmetry, thereby producing a wealth of specific phenomena that have been well identified in the past (spontaneous polarization, electronic work function, electronic surface states, surface polaritons, surface enhanced optical properties, ...).

In scanning probe microscopies, the currently used local probes give access to more and more accurate representations of the spatial distributions of a variety of surface near fields [2]. This progress is associated with a considerable improvement of the control of the tip-surface distance. However, rapid advances of the experimental techniques have increased the need for understanding how the signals detected by scanning probe microscopes are related to the various near fields which are known to be localized at the surface of materials [3].

In this Letter, we consider the specific example of the electron local density of states (LDOS). In the vicinity of a metal-vacuum interface, this quantity tails off exponentially into the vacuum and exhibits lateral oscillations around surface defects [4]. At the immediate proximity of close-packed surfaces of noble metal, these states can be probed using a scanning tunneling microscope (STM) [5–7]. Recently, the STM technique was applied to assemble circular corrals made of iron atoms adsorbed on the Cu(111) surface [5,6]. Subsequent STM images then showed that the electronic LDOS inside the corral revealed the electron eigenmodes sustained by the assembled structure. Several theoretical accounts of this experiment have been reported [8,9]. Specifically, based on the Green function method, a complete electron LDOS calculation associated with the corral geometry was performed by Crampin and Bryant [9].

In optics, the universal role played by the photonic LDOS in the proper description of surface optical phenomena was clearly identified in the past [10].

(i) For example, in the context of scanning near-field optical microscopy (SNOM) in illumination mode [11], it is observed experimentally that the images are not necessarily correlated to the underlying topography such as in a classical far-field microscope. A question still debated today deals with identifying the physical quantity which drives the variation of intensity in a SNOM experiment. The photonic LDOS might be the key to understanding such experiments.

(ii) The electromagnetic LDOS also appears as a constant factor in Planck's law of blackbody radiation. This constant factor counts only radiative eigenmodes. When dealing with realistic surfaces, nonradiative eigenmodes may also exist. They can also store energy, thereby affecting the thermal properties of surfaces. The optical corral is an example of tailoring such nonradiative eigenmodes.

(iii) The fluorescence of atoms and molecules is driven by the optical LDOS. It is thus possible to control the fluorescence signal of a set of atoms or molecules which would be deposited inside the corral relative to the reference level of the same amount of molecules which would be deposited outside the corral.

Well known as a main ingredient of the earliest theories of STM, the LDOS is not commonly used in electrodynamics [12,10]. In surface physics, the concept of LDOS $\rho(\mathbf{r}, \omega)$ is mostly applied to electrons so that $\rho(\mathbf{r}, \omega)d\mathbf{r}$ corresponds to the probability of finding an electron of energy $\hbar\omega$ in an infinitesimal volume $d\mathbf{r}$ centered at point \mathbf{r} above a surface. This scalar function is directly related to the square moduli of all possible electronic wave functions associated with this energy. In the case of photons, the most widely used formulation relies on the calculation

of the electric field susceptibility $\mathbf{G}(\mathbf{r}, \mathbf{r}, \omega)$ [12]. The physical link between $\rho(\mathbf{r}, \omega)$ and the response function $\mathbf{G}(\mathbf{r}, \mathbf{r}, \omega)$ is established as follows. We start from the probability to detect the intensity of the electric field associated with photons of energy $\hbar\omega$ at a given position \mathbf{r} :

$$\rho(\mathbf{r}, \omega) = \sum_n \delta(k_0^2 - k_n^2) |\mathcal{E}_n(\mathbf{r}, \omega_n)|^2, \quad (1)$$

where $k_0 = \omega/c$ and $\mathcal{E}_n(\mathbf{r}, \omega_n)$ represents the amplitude of the normalized electric field associated with the n th electromagnetic mode

$$\int |\mathcal{E}_n(\mathbf{r}, \omega_n)|^2 d\mathbf{r} = 1. \quad (2)$$

These modes obey the wave equation

$$-\nabla \wedge \nabla \wedge \mathcal{E}_n(\mathbf{r}, \omega_n) + k_n^2 \mathcal{E}_n(\mathbf{r}, \omega_n) = 0 \quad (3)$$

and a closure formula [\mathbf{I} is the unit dyadic and $\delta(\mathbf{r} - \mathbf{r}')$ is the Dirac delta function]

$$\sum_n \mathcal{E}_n(\mathbf{r}, \omega_n) \mathcal{E}_n^*(\mathbf{r}', \omega_n) = \mathbf{I} \delta(\mathbf{r} - \mathbf{r}'). \quad (4)$$

By using the well known representation of the Dirac delta function (Im denotes the imaginary part), we can write

$$\rho(r, \omega) = -\frac{1}{\pi} \lim_{\gamma \rightarrow 0} \sum_n \text{Im} \left(\frac{|\mathcal{E}_n(r)|^2}{k_0^2 - k_n^2 + i\gamma} \right). \quad (5)$$

From the equation which defines the field susceptibility

$$-\nabla \wedge \nabla \wedge \mathbf{G}(\mathbf{r}, \mathbf{r}', \omega) + k_0^2 \mathbf{G}(\mathbf{r}, \mathbf{r}', \omega) = -4\pi k_0^2 \mathbf{I} \delta(\mathbf{r} - \mathbf{r}') \quad (6)$$

and the above closure relation (4), we can deduce the spectral representation of \mathbf{G} as a function of the modal amplitudes \mathcal{E}_n :

$$\mathbf{G}(\mathbf{r}, \mathbf{r}', \omega) = -4\pi k_0^2 \sum_n \left(\frac{\mathcal{E}_n(\mathbf{r}, \omega_n) \mathcal{E}_n^*(\mathbf{r}', \omega_n)}{k_0^2 - k_n^2} \right). \quad (7)$$

By comparing the relations (7) and (5), we find

$$\rho(\mathbf{r}, \omega) = \frac{1}{4\pi^2 k_0^2} \text{Im}\{\text{Tr}\mathbf{G}(\mathbf{r}, \mathbf{r}, \omega)\}. \quad (8)$$

Let us note that this scalar quantity is the only quantitative way to describe the *continuous* part of the spectrum of any system independently of the excitation mode. In the context of optics, this means that the LDOS provides spectroscopic information which is intrinsically independent of any particular illumination mode. The main difficulty lies in the computation of the $\mathbf{G}(\mathbf{r}, \mathbf{r}, \omega)$ dyadic above the sample. When dealing with lithographically designed nanostructures deposited on a surface (cf. Fig. 1), the current developments of computation methods in real space provide powerful tools to derive the electromagnetic response $\mathbf{G}(\mathbf{r}, \mathbf{r}, \omega)$ [13]. Indeed, the field-susceptibility tensor can be computed by solving numerically a discretization of the Dyson equation:

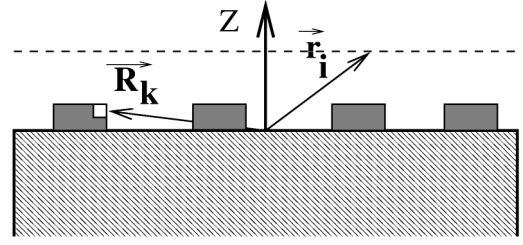


FIG. 1. Schematic drawing illustrating lithographically designed nanostructures on a transparent sample (dielectric constant $\epsilon_s = 2.25$). \mathbf{R}_k and \mathbf{r}_i represent, respectively, the positions of the discretization cells inside the source region (dielectric constant $\epsilon = n_{\text{pad}}^2 = 4.84$) and the positions explored in the observation plane.

$$\begin{aligned} \mathbf{G}(\mathbf{r}_i, \mathbf{r}_i, \omega) &= \mathbf{S}(\mathbf{r}_i, \mathbf{r}_i, \omega) \\ &+ \sum_{k=1}^n \chi_k(\mathbf{R}_k, \omega) \mathbf{S}(\mathbf{r}_i, \mathbf{R}_k, \omega) \\ &\cdot \mathbf{G}(\mathbf{R}_k, \mathbf{r}_i, \omega), \end{aligned} \quad (9)$$

where the source domain (i.e., the nanostructures) has been divided into n meshes centered at \mathbf{R}_k ($k = 1, \dots, n$) and where \mathbf{r}_i is any point in the observation plane. The size of each discretization cell V_k and the dielectric function $\epsilon(\mathbf{R}_k, \omega)$ of the nanostructures enters in the definition of

$$\chi_k(\mathbf{R}_k, \omega) = [\epsilon(\mathbf{R}_k, \omega) - 1] V_k / 4\pi. \quad (10)$$

In Eq. (9), \mathbf{S} represents the field susceptibility in the absence of nanostructures (i.e., associated with the bare plane surface). It is usually expressed as a sum of two contributions,

$$\mathbf{S}(\mathbf{r}, \mathbf{r}', \omega) = \mathbf{S}_0(\mathbf{r}, \mathbf{r}', \omega) + \mathbf{S}_{\text{surf}}(\mathbf{r}, \mathbf{r}', \omega), \quad (11)$$

where $\mathbf{S}_0(\mathbf{r}, \mathbf{r}', \omega)$ defines the free-space field susceptibility

$$\mathbf{S}_0(\mathbf{r}, \mathbf{r}', \omega) = [k_0^2 \mathbf{I} + \nabla_{\mathbf{r}} \nabla_{\mathbf{r}'}] \frac{e^{ik_0|\mathbf{r}-\mathbf{r}'|}}{|\mathbf{r}-\mathbf{r}'|}. \quad (12)$$

The contribution $\mathbf{S}_{\text{surf}}(\mathbf{r}, \mathbf{r}', \omega)$ is generated by the bare surface alone [13]. The numerical procedure described in [14] solves Dyson's equation (9) with high precision so that we can obtain reliable numerical data of the LDOS close to arbitrary nanostructures deposited on a surface.

In the absence of any sample, Eq. (9) reduces to $\mathbf{S}_0(\mathbf{r}, \mathbf{r}', \omega)$ [Eq. (12)], and the corresponding LDOS [Eq. (8)] simplifies to give

$$\rho_{\text{vacuum}}(\mathbf{r}, \omega) = \frac{k_0}{2\pi^2}, \quad (13)$$

namely, the familiar free-space electromagnetic LDOS (expressed in a k_0^2 unit) which enters Planck's blackbody radiation law. The presence of a lithographically designed sample locally modifies the density of available electromagnetic modes. This change of optical LDOS is defined by the *difference between the total and vacuum LDOS*:

$$\Delta\rho(\mathbf{r}, \omega) = \frac{1}{4\pi^2 k_0^2} \text{Im}\{\text{Tr}\mathbf{G}(\mathbf{r}, \mathbf{r}, \omega)\} - \frac{k_0}{2\pi^2}. \quad (14)$$

We have applied this technique (cf. Fig. 2) to visualize the evolution of the change of optical LDOS when gradually passing from a disordered geometry to a perfect circular corral. Each nanoscopic pad, of optical index $n_{\text{pad}} = 2.2$, is a truncated cylinder 100 nm high and 100 nm in diameter. The diameter of the final circular pattern is fixed at $3.6 \mu\text{m}$ (cf. Fig. 2c). Such *optical corrals* are feasible by current lithography techniques on a plane substrate.

In Fig. 2a we observe concentric rings around each individual pad. The change of optical LDOS increases strongly just above each pad. This spatial confinement of the electromagnetic LDOS is related to evanescent

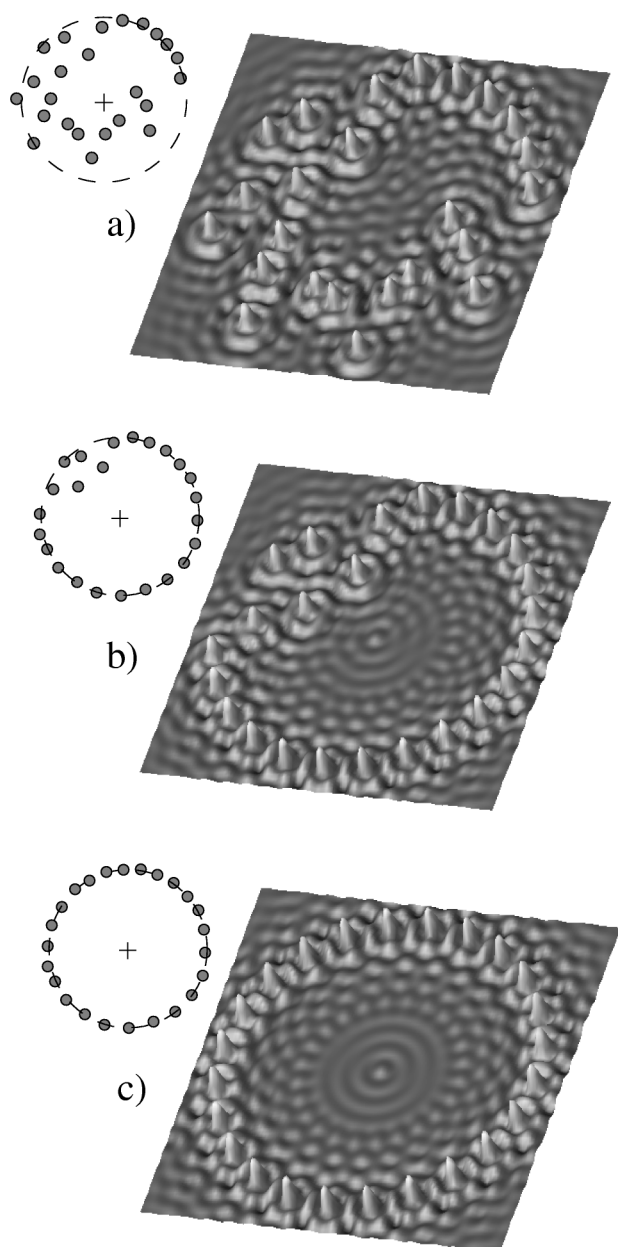


FIG. 2. Evolution of the change of optical LDOS $\Delta\rho(\mathbf{r}, \omega)$ when passing from disordered to ordered structures arranged to form a circular corral. The three calculations have been made at the wavelength $\lambda = 440 \text{ nm}$.

states generated by each individual pads. These particular states exist only in the near-field zone where they are produced by the nanostructures themselves. Mathematically, they mainly originate from the free space propagator $\mathbf{S}_0(\mathbf{r}, \mathbf{r}', \omega)$ [cf. Eq. (12)] that displays a r^{-3} short range behavior. Consequently, by increasing the change of optical LDOS in the very near-field zone, each pad allows high resolution to be achieved when observed with scanning near-field optical microscopes [11]. The period p of the fringe patterns surrounding the pads is merely related to the considered wavelength by the usual relation $p = \lambda/2 = \pi c/\omega$. This result points out a fundamental difference between optical and electron LDOS. In the case of electrons at the surface of a metal, the fringe period is inversely proportional to the square root of the surface electron effective mass. Figure 2c displays the change of the optical LDOS pattern above a perfectly circular array (so-called corral) of dielectric pads. In this simulation, the average diameter of the ring (pad center to pad center) is $3.6 \mu\text{m}$. The striking feature of this map is the strong modulation of the change of LDOS inside the corral that reflects the electromagnetic states sustained by the corral which are *localized at the surface*.

We now focus on the spectral properties of the optical corral of Fig. 2c. In Fig. 3, we present the variation of the change of optical LDOS, 50 nm above the surface, at the corral center, versus the wavelength in vacuum. The corresponding spectrum displays a series of resonant levels corresponding to the electromagnetic states associated with a circular truncated box. In spite of similarities with electrons near dense metal surfaces, some specific behavior occurs with light. Particularly, the smoothness of the *equivalent potential barrier* generated by standard dielectric materials can prevent a sufficient localization inside the corral. This effect can be compensated by using high optical index materials and by increasing the height of the structures.

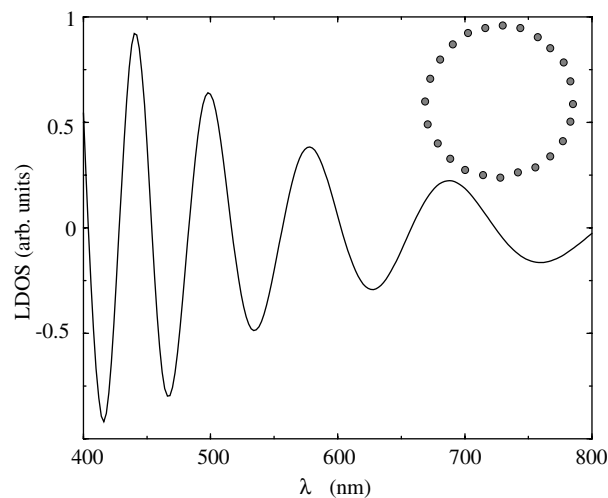


FIG. 3. Variation of the change of electromagnetic LDOS $\Delta\rho(\mathbf{r}, \omega)$ at the center of the corral versus the wavelength λ . Inside the corral a series of resonances can be identified.

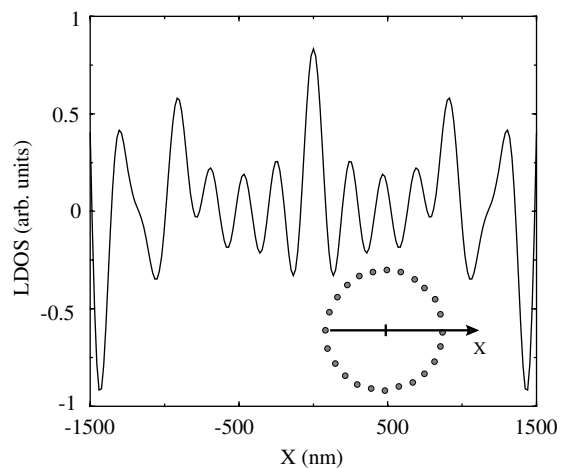


FIG. 4. Variation of the change of electromagnetic LDOS $\Delta\rho(\mathbf{r}, \omega)$ for a circular corral along the OX axis.

Figure 4 shows a crosscut of Fig. 2c. It displays more clearly the periodic oscillations as well as the shape of the central peak. This calculation has been performed at the first resonance of the LDOS spectrum (Fig. 3), i.e., for $\lambda = 440$ nm. If we compare this result with the solid curve of Fig. (2b) of Ref. [6], we note the strong analogy between the wavelike behavior of confined electrons and photons.

Unlike what happens with the usual STM imaging techniques, a direct measurement, in the visible range, of the optical LDOS requires a specific microscope design. At first sight, at least two issues should be considered.

(i) The first one relies on the analogy between electronic STM and photon scanning tunneling microscope (PSTM) [15]. In the electron STM, the presence of an isotropic electron gas under the surface of the metal enables a spontaneous incoherent excitation of all modal directions near the Fermi level to be achieved. In optics, to excite the complete change of LDOS, a modified version of the standard PSTM should include an isotropical incoherent illumination device that would allow all possible incident angles to be excited simultaneously. With this configuration, the wavelength dependence of the change of optical LDOS can be easily recorded by scanning the incident laser frequency.

(ii) A second method is based on the control of the fluorescence decay of an atom or a molecular level of energy $\hbar\omega_0$ [16]. Indeed, as proved by a recently published paper [17], near-field imaging of a sample with a single molecule has become possible. In a similar context, such pointlike detectors should provide optimal readings of the change of LDOS by locally measuring the fluorescence decay rate Γ_{ij} . Indeed, according to Fermi's golden rule, this quantity is given by [10]

$$\Gamma_{ij} \propto M_{ij}\rho(\mathbf{r}_m, \omega_0), \quad (15)$$

where M_{ij} is a matrix element that connects excited and fundamental states. Thus, for each position \mathbf{r}_m of the probing molecule with respect to the sample, the measurement of Γ_{ij} supplies a signal proportional to the change

of electromagnetic LDOS at the fluorescence frequency. Although, the validity range of Fermi's golden rule may become questionable in particular situations where local field effects are important [18] (i.e., in the presence of an optical cavity), the open surface system (the corral) considered here does not sustain high quality factor modes. Consequently, Eq. (15) remains reliable for a large range of molecule to surface distances [16].

In conclusion, we have performed full multiple-scattering calculations of the change of an electromagnetic LDOS near-surface structure of both arbitrary nature and profile. These calculations, based on solving numerically the dyadic Dyson equation, provide very stable numerical solutions, even for complex geometries. This analysis has allowed us to bring to the fore fundamental analogies and differences between electromagnetic waves and electrons confined by corral structures.

The authors acknowledge stimulating discussions with J. Weiner. In addition, we have benefited from the computing facilities provided by the center for massive parallel computing CALMIP of Toulouse. A.D. acknowledges financial support from the Regional Council of Burgundy.

-
- [1] A. Zangwill, *Physics at Surfaces* (Cambridge University Press, New York, 1988).
 - [2] H.-J. Güntherodt and R. Wiesendanger, *Theory of Scanning Tunneling Microscopy and Related Methods*, Springer Series in Surface Science (Springer, Berlin, 1993), 1st ed.
 - [3] C. Girard, C. Joachim, and S. Gauthier, Rep. Prog. Phys. **63**, 893 (2000).
 - [4] J. Tersoff and D. R. Hamann, Phys. Rev. B **31**, 805 (1985).
 - [5] M. F. Crommie, C. P. Lutz, and D. M. Eigler, Nature (London) **363**, 524 (1993).
 - [6] M. F. Crommie, C. P. Lutz, and D. M. Eigler, Science **262**, 218 (1993).
 - [7] J. Li, W. D. Schneider, R. Berndt, and S. Crampin, Phys. Rev. Lett. **80**, 3332 (1998).
 - [8] S. Crampin, M. H. Boon, and J. E. Inglesfield, Phys. Rev. Lett. **73**, 1015 (1994).
 - [9] S. Crampin and O. R. Bryant, Phys. Rev. B **54**, R17367 (1996).
 - [10] W. L. Barnes, J. Mod. Opt. **45**, 661 (1998).
 - [11] D. Courjon and C. Bainier, Rep. Prog. Phys. **57**, 989 (1994).
 - [12] G. S. Agarwal, Phys. Rev. A **11**, 230 (1975); *ibid.* **12**, 1475 (1975).
 - [13] C. Girard, A. Dereux, O. J. F. Martin, and M. Devel, Phys. Rev. B **52**, 2889 (1995).
 - [14] O. J. F. Martin, C. Girard, and A. Dereux, Phys. Rev. Lett. **74**, 526 (1995).
 - [15] R. C. Reddick, R. J. Warmack, and T. L. Ferrell, Phys. Rev. B **39**, 767 (1989).
 - [16] T. Pagnot, D. Barchiesi, D. Van Labeke, and C. Pieralli, Opt. Lett. **22**, 120 (1997).
 - [17] J. Michaelis, C. Hettich, J. Mlynek, and V. Sandoghdar, Nature (London) **405**, 325 (2000).
 - [18] P. de Vries, D. V. van Coevorden, and A. Lagendijk, Rev. Mod. Phys. **70**, 447 (1998).